Available online at www.sciencedirect.com
ScienceDirect
Journal of Nuclear Materials 362 (2007) 445–450
journal of nuclear materials
www.elsevier.com/locate/jnucmat

# Effect of gold ion irradiation on helium migration in fluoroapatites investigated with nuclear reaction analysis

S. Miro [a], F. Studer [a,*], J.-M. Costantini [b], P. Berger [c], J. Haussy [d], P. Trouslard [e], J.-J. Grob [f]

[a] *CRISMAT, ENSICAEN, 6 Bd du Maréchal Juin, F-14050 Caen cedex, France*
[b] *CEA Saclay, DMN/SRMA, F-91191 Gif-sur-Yvette cedex, France*
[c] *CEA Saclay, Laboratoire Pierre-Süe (CEA/CNRS), F-91191 Gif-sur-Yvette cedex, France*
[d] *CEA DIF, DCRE/SEIM, BP 12, F-91680 Bruyères-le-Châtel cedex, France*
[e] *CEA Saclay, LEMFI/INSTN/DRECAM, F-91191 Gif-sur-Yvette cedex, France*
[f] *CNRS-InESS, 23, rue du Loess, B.P. 20, F-67037 Strasbourg cedex, France*

## Abstract

In the context of nuclear waste storage, the knowledge of the effect of irradiation on the diffusion of helium produced by α-decays in apatites is an important issue. The analysis of implanted $^{3}He$ diffusion for two compositions was carried out with the $^{3}He(d,p)^{4}He$ nuclear reaction by using a deuteron milli- or micro-beam. Upon 163-MeV Au-ion irradiation, a significant fraction of $^{3}He$ atoms migrated towards the surface below which they were trapped, whereas a proportion of $^{3}He$ atoms remained trapped in the end-of-range region. Moreover, a clear helium loss was determined. These radiation-induced migration effects are enhanced in $Ca_{10}(PO_4)_6F_2$ compared with the $Ca_4Nd_6(SiO_4)_6F_2$.

*PACS:* 66.30.Jt; 61.72.Ss; 81.70.Jb; 24.30.v; 61.80.Jh; 61.82.Ms

## 1. Introduction

Apatites are considered to be potential matrices for nuclear waste storage. They form a large family of isomorphous compounds with the general chemical formula $Me_{10}(XO_4)_6Y_2$ which crystallizes in the hexagonal system (space group $P6_3/m$) [1]. The Me atoms and the $XO_4$ group stand for divalent cations and trivalent anions respectively. The charge is balanced by monovalent anions $Y^-$ ($Y = OH$, F). Apatitic structure flexibility versus substitution explains why the silicate substituted apatite, also known as britholite, can be used to store trivalent minor actinides ($Np^{3+}$, $Am^{3+}$, and $Cm^{3+}$) or fission products ($I^-$ and $Cs^+$) of $^{234}U$. The helium atoms produced by α-decays [2] will tend to diffuse, coalesce and form bubbles inducing detrimental modifications of the materials structure and mechanical properties [3]. Spontaneous fission, which is less probable, can create damage induced by electronic energy loss. It is thus of utmost importance to understand helium thermal diffusion, but also the

---

[*] Corresponding author. Tel.: +33 0 231452670; fax: +33 0 231951600.
*E-mail address:* francis.studer@ensicaen.fr (F. Studer).

0022-3115/$ - see front matter © 2007 Elsevier B.V. All rights reserved.
doi:10.1016/j.jnucmat.2007.01.214

radiation-enhanced diffusion (RED) of helium. In our previous study [4], we showed the influence of the chemical composition on the helium thermal diffusion process. The present study shows a clear RED effect induced by heavy-ion irradiation and the influence of the chemical composition thereof.

## 2. Experiments

The $Ca_{10}(PO_4)_6F_2$ and $Ca_4Nd_6(SiO_4)_6F_2$ ceramics were synthesized by a reactive sintering process described previously (for more details see Ref. [4–6]). The porosity values were 11.2 (4)% for $Ca_{10}(PO_4)_6F_2$ and 2.9 (3)% for $Ca_4Nd_6(SiO_4)_6F_2$. The porosity difference is in agreement with the SEM observations showing a denser compound in the case of $Ca_4Nd_6(SiO_4)_6F_2$ (Table 1(a)) than in the case of $Ca_{10}(PO_4)_6F_2$ (Table 1(b)) [4,5]. Samples were implanted with 3-MeV $^3He$ ions at a fluence of $10^{16}$ $cm^{-2}$ by using the Van de Graaff accelerator of the InESS laboratory (Strasbourg). Irradiation with 163-MeV Au ions at a fluence of $10^{12}$ $cm^{-2}$ was carried out at the VIVITRON facility (Strasbourg). The SRIM2000-code [7] parameters for the He ion implantation and the Au-ion irradiation are given in the Table 1. The $^3He$ depth profiles were determined with the $^3He(d,p)^4He$ nuclear reaction by using the milli-probe of van de Graaff accelerator of the INSTN (CEA/Saclay) and the micro-probe of the Laboratoire Pierre Süe (CEA/Saclay) with beam diameters of 1 mm and 2–3 μm respectively. The micro-beam was swept on a surface of 200 × 180 $\mu m^2$. More details on the experimental setup are available in Ref. [4]. The broad 'resonance' cross-section of this nuclear reaction (430 keV) is not adequate to obtain a good depth resolution for the $^3He$ depth profile [4]. Our solution was to sweep the deuteron beam energy gradually from 0.7 to 1.8 MeV, in order to shift the maximum of the cross-section inside the material. The proton yield was plotted on an excitation curve versus deuteron energy. This yield is the convolution of the $^3He$ depth profile with the nuclear reaction cross-section. Such a procedure was already used to study the thermal diffusion of $^3He$ in fluoroapatites [4,5,8] and zirconia [9].

## 3. Results

The excitation curves obtained with a micro-probe and milli-probe on the irradiated $Ca_4Nd_6(SiO_4)_6F_2$ sample are in very good agreement (Fig. 1(a)) within the experimental errors given by $\sqrt{I_0}$ ($I_0$ is the proton yield). The surface analyzed with the micro-probe is thus representative of the surfaces analyzed with the milli-probe. Fig. 1(b) obtained with the milli-probe shows the effect of composition. In both irradiated $Ca_{10}(PO_4)_6F_2$ and $Ca_4Nd_6(SiO_4)_6F_2$ samples, the excitation curves exhibit two bumps, one always centered around a deuteron energy (~1.2 MeV) corresponding to the $^3He$ end-of-range region (like the as-implanted

Table 1
Helium ion implantation and gold ion irradiation parameters for the two fluoroapatites: (a) $Ca_{10}(PO_4)_6F_2$ and (b) $Ca_4Nd_6(SiO_4)_6F_2$: projected ranges ($R_p$), longitudinal straggling ($\Delta R_p$), maximum displacements per atom (dpa) and electronic stopping powers

Table 1a

| Theoretical density (g $cm^{-3}$): 3.195 (3) | $Ca_{10}$ $(PO_4)_6F_2$<br>$^3He$ | Skeletal density (g $cm^{-3}$): 2.838 (9)<br>$^{197}Au$ |
|---|---|---|
| Energy (MeV) | 3 | 163 |
| Fluence ($cm^{-2}$) | $10^{16}$ | $10^{12}$ |
| $R_p$ (μm) | 10.40 | 15.40 |
| $\Delta R_p$ (μm) | 0.23 | 0.74 |
| $^3He$ peak concentration ($cm^{-3}$) | $1.85 \times 10^{20}$ (0.26 at.%) | – |
| Max dpa | 0.012 | $6.7 \times 10^{-4}$ |
| Electronic stopping power (keV $nm^{-1}$) | 0.21 | 20.0 |

Table 1b

| Theoretical density (g $cm^{-3}$): 4.869 (3) | $Ca_4$ $Nd_6$ $(SiO_4)_6F_2$<br>$^3He$ | Skeletal density (g $cm^{-3}$): 4.728 (9)<br>$^{197}Au$ |
|---|---|---|
| $R_p$ (μm) | 8.62 | 12.9 |
| $\Delta R_p$ (μm) | 0.30 | 0.95 |
| $^3He$ peak concentration ($cm^{-3}$) | $1.40 \times 10^{20}$ (0.19 at.%) | – |
| Max dpa | 0.016 | $1.05 \times 10^{-3}$ |
| Electronic stopping power (keV $nm^{-1}$) | 0.26 | 23.9 |

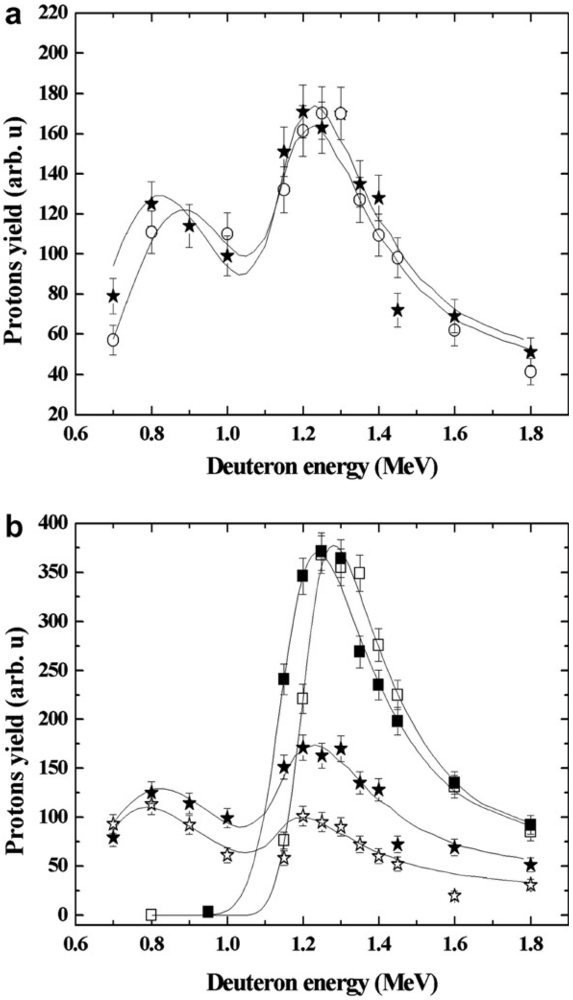

Fig. 1. Excitation curves obtained: (a) with the $^3He(d,p)^4He$ nuclear reaction by using the milli-probe (full star) and the micro-probe (open circle) for Au-ion irradiated $Ca_4Nd_6(SiO_4)_6F_2$, and (b) with the milli-probe for $Ca_4Nd_6(SiO_4)_6F_2$: as-implanted (full square) and Au-ion irradiated (full star), and for $Ca_{10}(PO_4)_6F_2$: as-implanted (open square) and Au-ion irradiated (open star). Solid lines are optimized with respect to the helium diffusion model.

excitation curve), called zone (**1**), and a second one closer to the surface, at lower energies, called zone (**2**) (Fig. 1(a) and (b)). This model allowed us to deduce the depths of both accumulation zones. Thus, with the milli-probe, we deduced that zone (**1**) lies at 2.6 μm below the surface for $Ca_{10}(PO_4)_6F_2$ composition and at 2.7 μm for $Ca_4Nd_6(SiO_4)_6F_2$ composition. Zone (**2**) lies at 7.2 μm below the surface for $Ca_{10}(PO_4)_6F_2$ composition and at 7.6 μm for $Ca_4Nd_6(SiO_4)_6F_2$ composition.

A fraction of the implanted $^3He$ atoms remained in zone (**1**) around which they could diffuse, and another part is found in zone (**2**). The first bump corresponding to zone (**1**) subsides more in the phosphate than in the silicate (Fig. 1(b)).

The mapping analysis achieved with the micro-probe (Fig. 2) reveals not only the above-mentioned in-depth heterogeneity of the $^3He$ profile, seen at different deuteron energies, but also a lateral heterogeneity depending also of depth. The mapping on as-implanted and irradiated $Ca_4Nd_6(SiO_4)_6F_2$ ceramics is shown in Fig. 2. Upon Au-ion irradiation (Fig. 2(a)), bright and dark zones are observed by optical microscopy (magnification 400×): they probably correspond to recrystallized areas and cracks respectively. These recrystallization phenomena were already observed by X-ray diffraction (XRD) at high electronic stopping power (≈19 keV $nm^{-1}$) with iodine ions (120 MeV) in $Ca_{10}(PO_4)_6F_2$ [6]. Such contrasts do not appear in the as-implanted sample (Fig. 2(b)). Actually, the black spots in Fig. 2(b) correspond to open micropores.

Contrary to the mapping of the as-implanted sample (Fig. 2(l)), $^3He$ atoms are detected at lower energies (0.8 MeV) in the irradiated sample (Fig. 2(k)), thus at lower depth corresponding to bright zones observed by optical microscopy (Fig. 2(a)), also called zone (**2**). This confirms that $^3He$ atoms are found closer to the surface. However, in the center of the mapping, a large $^3He$ concentration is still found at 1.2 MeV, corresponding to the end-of-range region (zone (**1**)). Some $^3He$ atoms thus remained trapped on the as-implanted profile. Lastly, the outer contours of the mapping correspond to dark zones, depleted by $^3He$ atoms, at any depth.

## 4. Discussion

The most probable assumption is that zone (**1**) corresponds to $^3He$ atoms trapped in the end-of-range region on defects produced by elastic collisions. These defects are distributed along the $^3He$ damage profile which is peaked at a depth ~near the projected range ($R_p \sim$ 8–9 μm) around which these $^3He$ atoms could diffuse. The other part of $^3He$ atoms migrated towards the surface in zone (**2**). These atoms are probably trapped beneath the crystals formed after recrystallization of the amorphous phase, as observed in optical microscopy (bright areas) and by XRD [6].

A diffusion model was developed to take these phenomena into account. This model is based

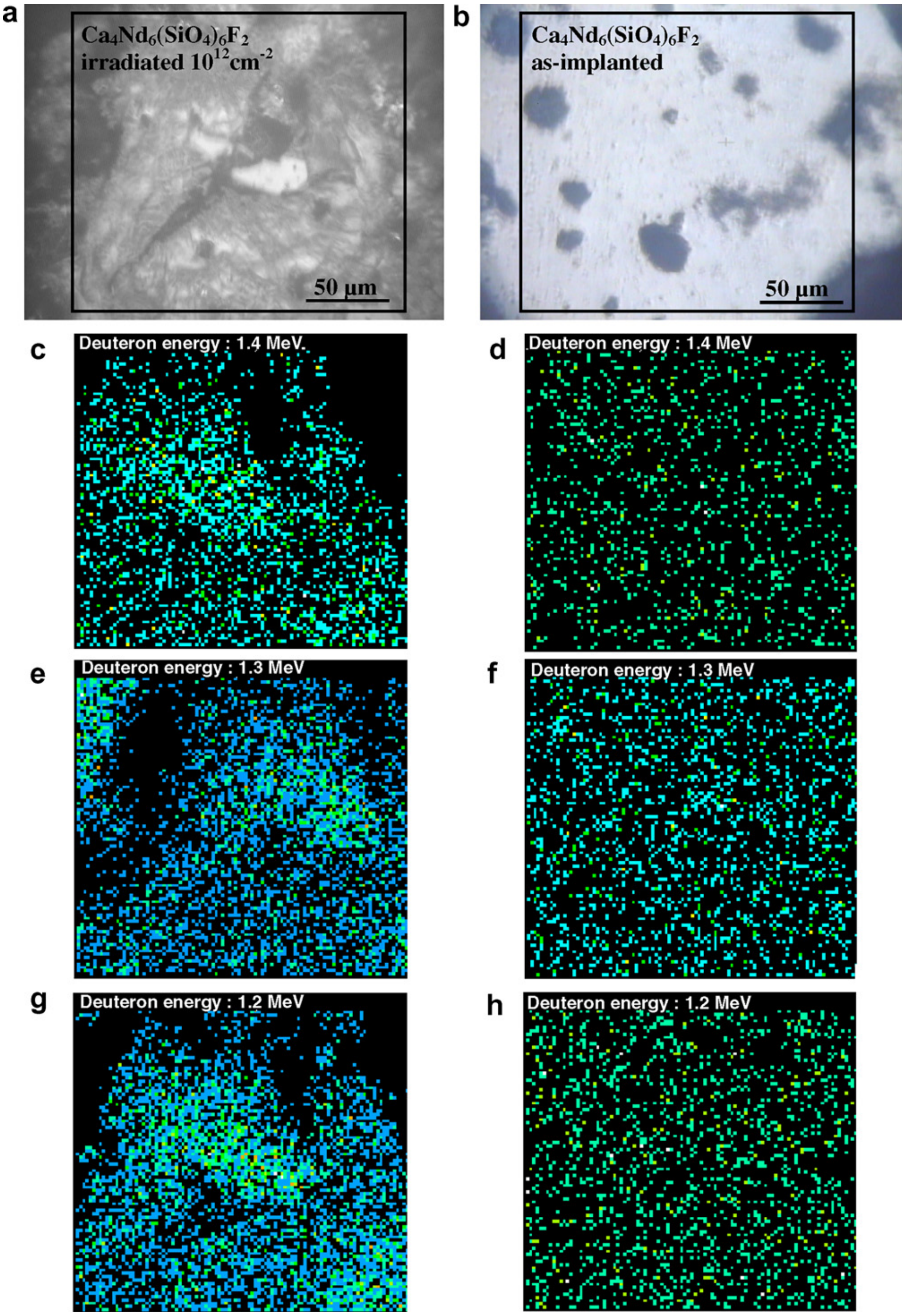

Fig. 2. (a) and (b) Optical micrographs and (c)–(n) $^3$He atom mapping carried out with the $^3$He(d,p)$^4$He nuclear reaction by using the micro-probe, for $Ca_4Nd_6(SiO_4)_6F_2$: Au-ion irradiated (left), and as-implanted (right). The square boxes on the micrographs indicate the approximate boundaries of the mapping analysis. On $^3$He atom mapping pictures, each white dot corresponds to the proton yield coming out of the sample after the nuclear reaction $^3$He(d,p)$^4$He. At a given deuteron energy corresponds an Helium density at a depth which can be estimated from SRIM calculations: for instance zone (**1**) (Fig. 1(a)), which lies at 2.7 μm for $Ca_4Nd_6(SiO_4)_6F_2$, corresponds to 0.8 MeV deuteron energy. Zone (**2**), which lies at 7.6 μm below the surface for $Ca_4Nd_6(SiO_4)_6F_2$, corresponds to 1.3 MeV deuteron energy.

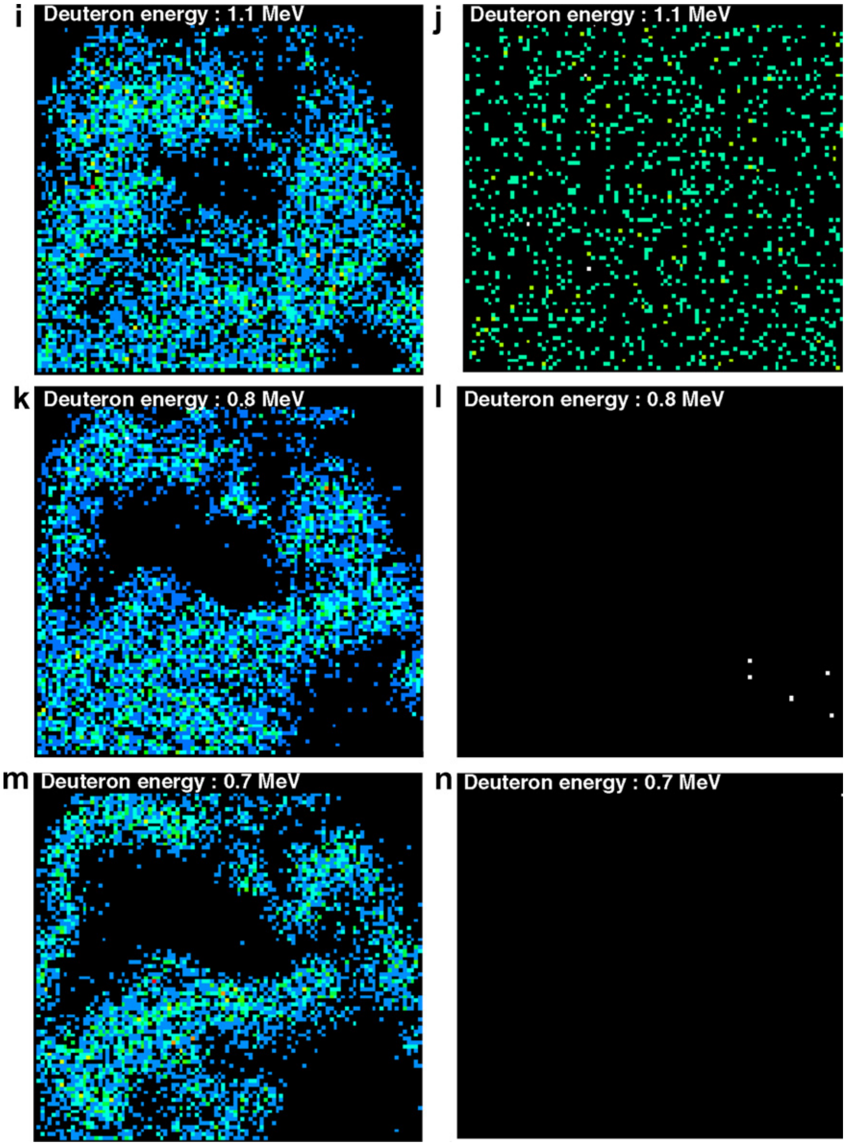

Fig. 2 (*continued*)

on equations similar to the model previously used for thermal diffusion [4]. In the latter model, the detected proton yield $I_0(E_0)$ at a given incident deuteron energy $E_0$ is the convolution of the $^3$He depth profile with the cross-section of the nuclear reaction $^3$He(d,p)$^4$He [10]:

$$I_0(E_0) = \int_0^{x_0} \sigma(E(x))\rho(x)\mathrm{d}x, \qquad (1)$$

where $x_0$ is the deuteron projected range, $\sigma$ is the cross section, $E(x)$ is the deuteron energy at depth $x$ (data given by the SRIM 2000 code [7]), and $\rho(x)$ is the $^3$He depth profile. Details on the fitting process for the excitation curves are given in Ref. [4]. The difference with the previous model is that we assume the existence of two accumulation zones, with two $^3$He depth profiles, $\rho_1(x)$ in zone (**1**) and $\rho_2(x)$ in zone (**2**),in order to fit the experimental excitation curves. Details of this new model will be published elsewhere. It is seen that the optimized excitation curves reproduce well the shapes of experimental curves (Fig. 1(a) and (b)). Moreover, the optimized parameters of the model show that there is no conservation of the $^3$He content for both compositions after irradiation, with a sizable helium loss: 54% for $Ca_{10}(PO_4)_6F_2$ and 28% for $a_4Nd_6(SiO_4)_6F_2$. This means that the remaining $^3$He atoms have been redistributed in the bulk of the solid into two definite distributions peaked at two well defined depths corresponding to the above-mentioned zones (**1**) and (**2**). This NRA technique had already allowed us to detect $^3$He loss out of the profile in cubic yttria-stabilized zirconia ($ZrO_2$ : Y) upon annealing at 1073 K [9].

The clear helium loss inferred from the NRA data is quite consistent with the rugged surface of the irradiated samples with apparent cracks (Fig. 2(a)). Helium out-gassing was indeed expected since the optical micrographs seem to show that blister bursts have occurred at the surface. Blistering and exfoliation were also observed in the case of $^4$He implantation in $Ca_{10}(PO_4)_6F_2$ single crystals at a lower energy (1.6 MeV) and a critical concentration about 5 at.% [11,12], which is much smaller than that found in metals and semiconductors ($\sim$20 at.%) [3]. However, such effects were not found in sintered ceramics with the same composition at a $^4$He peak concentration about 10 at.%, due to helium pipe diffusion to the surface along micro-channels [11,12].

With a much lower $^3$He content ($\sim$0.4 at.% peak concentration) and deeper end-of-range region, we did not observe such effects of helium loss and blistering/exfoliation in the case of thermal diffusion in sintered fluoroapatites up to 673 K during 1 h [4]. The present RED of helium and crater formation at such a low concentration is thus likely due to the amorphization and recrystallization processes induced by the high electronic energy loss along the heavy-ion path [5,6]. The radiation-enhanced helium migration towards the surface was certainly impeded by the presence of recrystallized areas which may act as diffusion barriers. Nevertheless, further experiments with different heavy-ion irradiation conditions such as stopping power and fluence are needed to confirm the RED effect seen with these data.

## 5. Conclusion

To study the diffusion of helium in fluoroapatites, analyses of implanted $^3$He depth profiles were carried out with the $^3$He(d,p)$^4$He nuclear reaction by using a deuteron milli- or micro-beam. Upon 163-MeV Au-ion irradiation, two bumps were observed in the plots of the proton yield versus deuteron energy between 0.2 and 1.8 MeV. We assume that a part of $^3$He atoms remained centered in the end-of-range region, trapped on defects produced by the elastic collisions. A significant fraction of $^3$He atoms migrated towards the surface, one part escaping from the solid, and another one being trapped below the surface, probably under recrystallized zones. This is interpreted as a RED of helium which increases in the phosphate with respect to the silicate.

## References

[1] C. Rey, L'actualité Chimique (1995) 41.
[2] W.J. Weber, R.C. Ewing, A. Meldrum, J. Nucl. Mater. 250 (1997) 147.
[3] S.E. Donnelly, J.H. Evans (Eds.), Fundamentals of Inert Gases in Solids, Plenum, New York, 1991.
[4] S. Miro, F. Studer, J.M. Costantini, J. Haussy, P. Trouslard, J.J. Grob, J. Nucl. Mater. 355 (2005) 1.
[5] S. Miro, Caen University Thesis, 2003.
[6] S. Miro, D. Grebille, D. Chateigner, D. Pelloquin, J.-P. Stoquert, J.-J. Grob, J.-M. Costantini, F. Studer, Nucl. Instrum. Meth. B 227 (2005) 306.
[7] J.P. Biersack, L.G. Haggmark, Nucl. Instrum. and Meth. 174 (1980) 257.
[8] J.-M. Costantini, P. Trocelier, J. Haussy, J.-J. Grob, Nucl. Instrum. and Meth. B 195 (2002) 400.
[9] J.-M. Costantini, J.-J. Grob, J. Haussy, P. Trocellier, P. Trouslard, J. Nucl. Mater. 321 (2003) 281.
[10] M.B. Lewis, N.H. Packan, G.F. Wells, R.A. Buhl, Nucl. Instrum. and Meth. B 167 (1979) 233.
[11] S. Soulet, Orsay University Thesis, 2000.
[12] S. Soulet, J. Carpéna, J. Chaumont, O. Kaitasov, M.-O. Ruault, J.-C. Krupa, Nucl. Instrum. and Meth. B 184 (2001) 383.